Generalized Optimization of Sparse Antenna Arrays for High-Resolution Automotive Radar Imaging

Lifan Xu[†], Shunqiao Sun[†], Ryan Wu[‡], Dongyin Ren[‡], and Jun Li[‡]

[†]Department of Electrical and Computer Engineering, The University of Alabama, Tuscaloosa, AL 35487 [‡]NXP Semiconductors, San Jose, CA 95134

Abstract-Automotive radar with sparse arrays are highly desired, as a sparse array has a smaller number of elements compared to a uniform linear array (ULA) of the same physical aperture size, resulting in lower system cost, increased flexibility, and reduced mutual coupling between antennas. However, this leads to an increase in sidelobes in the angle spectrum and higher signal processing complexity. Interpolation techniques can help reduce sidelobe levels, mitigating ambiguity in angle estimation with sparse arrays, and improving the ability to distinguish desired signals from interference. In this paper, we investigate transform matrix optimization technique to interpolate a virtual sparse array (VSA) synthesized by automotive multi-input multi-output (MIMO) radar to a ULA so that high-resolution direction-of-arrival estimation algorithms that are designed for ULA can be applied to VSA to achieve highresolution radar imaging. Our simulation results in the one dimensional (1D) sparse arrays demonstrate the feasibility and effectiveness of this technique.

Index Terms—Automotive radar, sparse array, array interpolation, direction-of-arrival estimation

I. INTRODUCTION

Autonomous driving requires accurate and reliable detection of objects, including vehicles, pedestrians, and obstacles, in the highly dynamic environment. Radar-based sensing systems are one of the most commonly used technologies for object detection in autonomous driving due to their ability to provide accurate distance and velocity measurements regardless of lighting and weather conditions [1, 2]. In radar-based sensing systems, sparse arrays can achieve a larger antenna array aperture by deploying antenna elements in a non-uniform spacing pattern, offering higher resolution while maintaining a lower cost over the uniform linear array with half wavelength spacing and same number of antenna elements [2].

The phase discontinuity nature of sparse arrays would result in high sidelobes, presenting a challenge for resolving targets' angles. Compressed sensing (CS) can be applied for angle estimation on sparse arrays. However, the construction of the CS dictionary and solving the relaxed l_1 norm optimization problem is of high computational cost. Further, CS suffers from off-grid issue [3, 4]. Subspace based super resolution angle finding methods, such as MUSIC and ESPRIT, are suitable for well-structured sparse arrays [5]. For example, to apply ESPRIT, the sparse arrays may consist of multiple identical shifted sparse subarrays that satisfying the rank properties [6], and careful angle unfolding design is required to mitigate the angle ambiguity due to large shift among subarrays [5]. However, applying the subspace methods to coherent signals can be difficult, since it is challenging to apply the spatial smoothing technique to sparse arrays [6]. The popular difference coarrays, such as nested array [7] and coprime array [8], can resolve the number of targets that is much larger than the number of physical array elements. However, these difference coarrays rely on the accurate estimation of the array covariance matrix, which requires a large number of snapshots in a wide-sense stationary (WSS) process scenario [7, 9], which is a big challenge

in highly dynamic automotive scenarios [10, 11]. In addition to sparse array angle finding, machine learning can also be used to identify patterns and relationships in received data. This method involves training a machine learning model on a large dataset to learn the relationship between received signals and angles of arrival. The model can then estimate the angle of arrival of new signals [12–14]. However, a large number of training datasets are required for this method to work effectively. Insufficient training data may lead to poor generalization performance and biased estimated results.

The array response of a uniform linear array (ULA) has a Vandermonde structure, which is crucial for applying many essential angle estimation algorithms. Thus, it is desired to transform a sparse array into a uniform linear array with interpolation techniques. This transformation enables the use of algorithms that are designed for uniform linear arrays, such as the matrix pencil [15], for angle estimation in sparse arrays. Numerous interpolation techniques are available for the recovery or approximation of missing data in sparse datasets, such as transformation matrices [16-19], linear regression [20], and matrix completion methods [2, 21-24]. The linear regression method, in particular, is effective for non-random sparse arrays, which demands a homogeneous linear model capable of predicting coefficients for missing data. On the other hand, the matrix transformation method is typically well-suited for scenes with a limited field of view (FOV) due to the necessity for discretization. Excessively large FOVs can result in diminished interpolation accuracy. The matrix completion method offers flexibility in designing sparse array geometries to facilitate the filling of missing elements. However, its computational cost is notably high, primarily attributed to the singular value decomposition (SVD) operation in each iteration [25].

In this paper, we investigate the sparse array interpolation for automotive MIMO radar using transform matrix. The automotive MIMO radar is first optimized to have minimal peak sidelobe level. Subsequently, various approaches are investigated to design the optimal transform matrix to interpolate a virtual sparse array (VSA) into a ULA. To improve the interpolation performance, the array FOV is divided into multiple sectors, and array interpolation is carried out sector-by-sector. The out-of-sector suppression is considered in the sector-based interpolation optimization to minimize high sidelobe in the out-of-sector regions. The effectiveness of the virtual sparse array interpolation is verified through numerical results.

II. SYSTEM MODEL OF AUTOMOTIVE MIMO RADAR

Let's consider K narrow-band, far-field signals impinging onto a one dimensional (1D) colocated sparse multi-input and multi-output (MIMO) array with N transmitters and M receivers, located at dt_n for $n=1,2,\cdots,N$ and dr_m for $m=1,2,\cdots,M$, respectively. Define $\mathbb{D}_t=\{dt_1,\cdots,dt_N\}$ and $\mathbb{D}_r=\{dr_1,\cdots,dr_M\}$. Assume the transmit waveform from different transmitters are orthogonal so

Asilomar 2023

that the contribution of each transmitter can be easily separated at the receive antenn array using matched filter.

The received data matrix $\mathbf{Y} \in \mathbb{C}^{M \times N}$ can be written as [26]

$$\mathbf{Y} = \mathbf{A}_r \mathbf{S} \mathbf{A}_t^T + \mathbf{W},\tag{1}$$

where $\mathbf{A}_t \in \mathbb{C}^{N \times K}$ and $\mathbf{A}_r \in \mathbb{C}^{M \times K}$ are the transmit and receive array steering matrices with $\mathbf{A}_t = [\mathbf{a}_t(\theta_1), \mathbf{a}_t(\theta_2), \cdots, \mathbf{a}_t(\theta_K)]$ and $\mathbf{A}_r = [\mathbf{a}_r(\theta_1), \mathbf{a}_r(\theta_2), \cdots, \mathbf{a}_r(\theta_K)]$, respectively. Here, the transmit and receive array steering vectors are

$$\mathbf{a}_{t}(\theta_{k}) = \left[e^{j\frac{2\pi}{\lambda}dt_{1}\sin(\theta_{k})}, \cdots, e^{j\frac{2\pi}{\lambda}dt_{N}\sin(\theta_{k})}\right]^{T}, \tag{2}$$

$$\mathbf{a}_r(\theta_k) = \left[e^{j\frac{2\pi}{\lambda} dr_1 \sin(\theta_k)}, \cdots, e^{j\frac{2\pi}{\lambda} dr_M \sin(\theta_k)} \right]^T.$$
 (3)

The diagonal matrix $\mathbf{S} = \mathrm{diag}\{[\beta_1, \cdots, \beta_K]\}$ contains the target's radar cross-section (RCS), and \mathbf{W} is the noise matrix. The receive data matrix can be rearranged as a long vector $\mathbf{y} \in \mathbb{C}^{MN \times 1}$ through vectorization, i.e.,

$$\mathbf{y} = \operatorname{vec}(\mathbf{Y}) = \mathbf{A}_t \otimes \mathbf{A}_r \operatorname{vec}(\mathbf{S}) + \operatorname{vec}(\mathbf{W}).$$
 (4)

Here, \otimes denotes the Kronecker product. Noting that matrix **S** is diagonal, we can rewrite equation (4) as

$$y = As + w, (5$$

where $\mathbf{A} = [\mathbf{a}(\theta_1), \cdots, \mathbf{a}(\theta_K)] \in \mathbb{C}^{MN \times K}$ is the virtual array manifold, with $\mathbf{a}(\theta_k) = \mathbf{a}_t(\theta_k) \otimes \mathbf{a}_r(\theta_k)$. Here, $\mathbf{s} = [\beta_1, \cdots, \beta_K]^T$ and $\mathbf{w} = \text{vec}(\mathbf{W})$. It can be verified that automotive MIMO radar achieves a large virtual array aperture with MN elements using only N transmit and M receive antennas, thus saving the hardware cost.

To further reduce the hardware cost, we aim to design automotive MIMO radar by exploiting sparse arrays. In automotive MIMO radar, the sparse array design boils down to select N transmit antennas from a ULA with N_T array elements, and M receive antennas from a ULA with M_R elements. Here, $M_T > M$ and $N_T > N$. Assume the field of view of virtual array is $[-\theta_c, \theta_c]$. The main beam is within the region Ω_p of $[-\theta_p, \theta_p]$, and the main beam width is determined by the virtual array aperture. Consequently, the sidelobe region Ω_s is $[-\theta_c, -\theta_p) \cup (\theta_p, \theta_c]$.

The resulting irregular virtual sparse array (VSA) has high sidelobe, which may introduce ambiguity for direction-of-arrival estimation. The positions of VSA elements are

$$\bar{\mathbf{d}} = [dt_1 + dr_1, \cdots, dt_1 + dr_M, \cdots, dt_N + dr_M] \in \mathbb{R}^{MN \times 1}.$$

Assume the MIMO transmit and receive arrays are designed such that there are no repeated values in $\bar{\mathbf{d}}$. In other words, all the values of $\bar{\mathbf{d}}$ are unique. Let $\mathbf{d} = [d_1, \cdots, d_{MN}]$ denote the sorted positions of VSA elements $\bar{\mathbf{d}}$ in an increasing order, where $d_i, i=1,\cdots,MN$ are the positions of the i-th virtual element. The aperture of VSA is $D = d_{MN} - d_1$. The array manifold of the VSA is

$$\mathbf{a}_{\mathrm{VSA}}\left(\theta_{k}\right) = \left[e^{j\frac{2\pi}{\lambda}d_{1}\sin(\theta_{k})}, e^{j\frac{2\pi}{\lambda}d_{2}\sin(\theta_{k})}, \cdots, e^{j\frac{2\pi}{\lambda}d_{MN}\sin(\theta_{k})}\right]^{T}.$$
(7)

To overcome the challenge associated with VSA, we aim to interpolate the VSA into a ULA with the same aperture and element spacing of half-wavelength $d=\lambda/2$. The array manifold of the interpolated ULA is

$$\mathbf{a}_{\text{ULA}}\left(\theta_{k}\right) = \left[1, e^{j\frac{2\pi}{\lambda}d\sin(\theta_{k})}, \cdots, e^{j\frac{2\pi}{\lambda}(Q-1)d\sin(\theta_{k})}\right]^{T}, \quad (8)$$

where Q is the number of elements in ULA and $Q = 2D/\lambda > MN$.

III. SPARSE ARRAY INTERPOLATION OPTIMIZATION

The virtual sparse array is first optimized to have minimal peak sidelobe level (PSL) before carrying out interpolation. Transform matrix is then introduced to interpolate the optimized virtual sparse array into a uniform linear array with the same aperture. To enhance the interpolation result, the entire FOV is typically divided into multiple sectors, and interpolation is done sector-by-sector.

A. Sparse Array Peak Sidelobe Level Optimization

Interpolation of a sparse virtual array with minimal PSL can yield better results than interpolating a randomly generated sparse array. Therefore, before carrying out the array interpolation, it is desired to optimize the sparse virtual array geometry such that its PSL is minimized [27]. The array factor (AF) of the virtual sparse array is

$$AF\left(\theta, \mathbb{D}_{t}, \mathbb{D}_{r}\right) = \sum_{i=1}^{MN} e^{j2\pi d_{i}\sin(\theta)}.$$
 (9)

Then, the peak sidelobe level (PSL) of the virtual array is defined as

$$PSL = \max_{\theta \in \Omega_s} 20 \log |AF(\theta, \mathbb{D}_t, \mathbb{D}_r)|.$$
 (10)

Numerically, the PSL can be calculated by discretizing the sidelobe region Ω_s with step size of $\Delta\theta$ and the maximum value of the array factor in the sidelobe region is defined as PSL. Here, $\Delta\theta$ represents the angle resolution determined by the virtual array aperture size. Sparse array optimization aims to minimize the PSL by adjusting the antenna positions \mathbb{D}_t , \mathbb{D}_r , i.e.,

$$\min_{\mathbb{D}_{t}, \mathbb{D}_{r}} \max_{\theta \in \Omega_{s}} 20 \log |AF(\theta, \mathbb{D}_{t}, \mathbb{D}_{r})|. \tag{11}$$

The transmit and receive antennas positions \mathbb{D}_t , \mathbb{D}_r can be interleaved. In practice, it is imperative that all transmit and receive arrays are within the feasible aperture size D with minimal separation of Δ for antenna fabrication and reduction of mutual coupling. The PSL minimization problem considering the minimal separation among physical transmit and receive antennas are formulated as

$$\begin{aligned} \min_{\mathbb{D}_{t},\mathbb{D}_{r}} \max_{\theta \in \Omega_{s}} 20 \log |AF\left(\theta, \mathbb{D}_{t}, \mathbb{D}_{r}\right)| \\ \text{s.t.} \quad |dt_{n} - dt_{l}| \geq \Delta, \quad \forall \ dt_{n} \in \mathbb{D}_{t}, \forall \ dt_{l} \in \mathbb{D}_{t}, n \neq l \\ \left| dr_{m} - dr_{p} \right| \geq \Delta, \quad \forall \ dr_{m} \in \mathbb{D}_{r}, \forall \ dr_{p} \in \mathbb{D}_{r}, m \neq p \\ \left| dt_{n} - dr_{m} \right| \geq \Delta, \quad \forall \ dt_{n} \in \mathbb{D}_{t}, \forall \ dr_{m} \in \mathbb{D}_{r} \end{aligned}$$

$$(12)$$

The PSL optimization problem is challenging to solve, especially if the locations of the transmit and receive antennas are on-grid with grid size of half wavelength. Usually, heuristic algorithms such as particle swarm optimization [28] can be applied to speed up the search process [29].

B. Sparse Array Interpolation with Transform Matrix

A transform matrix $\mathbf{T} \in \mathbb{C}^{Q \times MN}$ can be utilized to interpolate the VSA into a ULA [16]. Mathematically, the transform matrix is designed such that

$$\mathbf{Ta}_{\mathrm{VSA}}(\theta_k) \cong \mathbf{a}_{\mathrm{ULA}}(\theta_k), \quad \forall \theta_k \in [-\theta_c, \theta_c].$$
 (13)

The matrix T serves as a calibration dictionary.

To obtain the transform matrix \mathbf{T} , we define the cost function C as follows

$$C = \int \| \mathbf{T} \mathbf{a}_{VSA}(\theta_k) - \mathbf{a}_{ULA}(\theta_k) \|_2 \ \omega(\theta) d\theta$$
 (14)

where the $\omega(\theta)$ is the weighting. Closed-form solutions, such as least square (LS) and the singular value decomposition (SVD), can be employed to obtain the transform matrix ${\bf T}$ by minimizing the cost

function C [27]. Additionally, convex optimization methods can also be applied to obtain the transform matrix \mathbf{T} [30].

1) Least square closed-form solution: The least square solution of obtaining transform matrix T by minimizing the cost function C is given by [27] $T = FG^{-1}$, where

$$\mathbf{F} = \int \mathbf{a}_{\text{ULA}}(\theta) \mathbf{a}_{\text{VSA}}^{H}(\theta) \omega(\theta) d\theta,$$

$$\mathbf{G} = \int \mathbf{a}_{\text{VSA}}(\theta) \mathbf{a}_{\text{VSA}}^{H}(\theta) \omega(\theta) d\theta.$$
(15)

To ensure the invertibility of **G** and mitigate instability, particularly when the condition number is too large, one approach is to minimize its condition number. The condition number is related to the sparsity of the array, i.e., the number of antenna elements, and the sparse array geometry.

2) Optimization toolbox solution: The array FOV can be discretized with a small angle step $\Delta\theta$, resulting in the interpolated set

$$\Omega = \{ -\theta_c, -\theta_c + \Delta\theta, -\theta_c + 2\Delta\theta, \dots, \theta_c \}$$

with cardinality of $P=\frac{2\theta_c}{\Delta\theta}+1.$ The array manifolds corresponding to the VSA and ULA are denoted by

$$\mathbf{A}_{\text{VSA}} = [\mathbf{a}_{\text{VSA}}(-\theta_c), \mathbf{a}_{\text{VSA}}(-\theta_c + \Delta\theta), \cdots, \mathbf{a}_{\text{VSA}}(\theta_c)], \mathbf{A}_{\text{ULA}} = [\mathbf{a}_{\text{ULA}}(-\theta_c), \mathbf{a}_{\text{ULA}}(-\theta_c + \Delta\theta), \cdots, \mathbf{a}_{\text{ULA}}(\theta_c)].$$
(17)

The transform matrix T is designed such that

$$\mathbf{T}\mathbf{A}_{\mathrm{VSA}} \cong \mathbf{A}_{\mathrm{ULA}}.$$
 (18)

Matrix T is obtained by minimizing the interpolation error under Frobenius norm, i.e.,

$$\min_{\mathbf{T}} \parallel \mathbf{T} \mathbf{A}_{\text{VSA}} - \mathbf{A}_{\text{ULA}} \parallel_F. \tag{19}$$

The CVX toolbox [31] can be applied to solve the optimization problem (19) efficiently.

3) Rotational signal subspace solution: It has been shown that a good transform matrix is unitary [32]. Therefore, the transform matrix T is obtained by minimizing the Frobenius norm of the interpolation error subject to a unitary constraint, i.e.,

$$\min_{\mathbf{T}} \| \mathbf{T} \mathbf{A}_{\text{VSA}} - \mathbf{A}_{\text{ULA}} \|_{F}$$
s.t.
$$\mathbf{T}^{H} \mathbf{T} = \mathbf{I}$$
(20)

Sparse array interpolation using the transform matrix will rotate the narrow-band signal subspace spanned by $\{A_{\rm VSA}\}$ so that it is close to the narrow-band signal subspace spanned by $\{A_{\rm ULA}\}$ in the Frobenius norm sense. The rotational signal subspace solution [32] of matrix T is given as

$$\mathbf{T} = \mathbf{V}\mathbf{U}^H,\tag{21}$$

where $\mathbf{U} \in \mathbb{C}^{MN \times P}$ and $\mathbf{V} \in \mathbb{C}^{Q \times P}$ are left and right singular vectors of matrix $\mathbf{A}_{\text{VSA}} \mathbf{A}_{\text{ULA}}^H$, i.e.,

$$\mathbf{A}_{\mathrm{VSA}}\mathbf{A}_{\mathrm{ULA}}^{H} = \mathbf{U}\Sigma\mathbf{V}^{H}.$$
 (22)

C. Sector-Based Transform Matrix Design

It is challenging to have a single transform matrix $\mathbf T$ that works well for the whole discretized FOV set Ω . Instead, the whole FOV can be divided into N_s sectors $\Psi_i \subset \Omega$ for $i=1,\cdots,N_s$. Then interpolation is carried out sector-by-sector. For sector-based interpolation, the challenges lie in the impact of out-of-sector sources. Without suppression of the sources out of the interpolated sector, it can notably impact angle-finding performance.

A mask matrix, $\mathbf{M} \in \mathbb{R}^{Q \times P}$, can be adopted to control the interpolation response of both in-sector and out-of-sector. With the mask matrix, the interpolation problem (19) is updated as

$$\min_{\mathbf{T}} \| \mathbf{T} \mathbf{A}_{\text{VSA}} - \mathbf{M} \odot \mathbf{A}_{\text{ULA}} \|_{F}, \tag{23}$$

where ⊙ denotes the Hadamard product. The design of the mask matrix M is flexible, provided it satisfies the following requirements: (i) the ability to suppress out-of-sector signals to facilitate effective sector-by-sector processing, and (ii) the columns of M corresponding to the in-sector region are set to 1, a vector with all elements as 1, implying that the in-sector response should be the same as the ULA. The sector-based transform matrix can be obtained by solving the optimization problem of (23) using CVX toolbox.

An alternative approach to mitigate the influence of signals from the out-of-sector is to reformulate equation (23) as

$$\min_{\mathbf{T}} \max_{m} \parallel \mathbf{T} \mathbf{a}_{\mathrm{VSA}}(\theta_{m}) - \mathbf{a}_{\mathrm{ULA}}(\theta_{m}) \parallel_{p}, \ \theta_{m} \in \Psi_{i}$$
s.t. $\parallel \mathbf{T} \mathbf{a}_{\mathrm{VSA}}(\theta_{k}) \parallel_{p} \leq \gamma, \ \theta_{k} \in \Phi$ (24)

Here, Ψ_i and Φ denote the i-th in-sector and out-of-sector, respectively. The positive small number γ quantifies the out-of-sector interpolation attenuation. When p-norm is replaced with l_2 -norm, the optimization problem (24) becomes a convex quadratically constrained quadratic programming (QCQP) problem, which can be solved efficiently using the CVX toolbox.

However, it is difficult to achieve a flat interpolation error over the in-sector region under l_2 -norm in problem (24). It is shown that opting for l_1 -norm for interpolation error and l_{∞} -norm for out-of-sector attenuation in (24) allows for bounding the interpolation error [33]. The new optimization problem is

$$\min_{\mathbf{T}} \max_{k} \| \mathbf{T} \mathbf{a}_{VSA}(\theta_{k}) \|_{\infty}, \ \theta_{k} \in \Phi$$
s.t. $\| \mathbf{T} \mathbf{a}_{VSA}(\theta_{m}) - \mathbf{a}_{ULA}(\theta_{m}) \|_{1} \le \varepsilon, \ \theta_{m} \in \Psi_{i}$ (25)

Here, ε denotes the predefined interpolation error level. The optimization problem (25) can be casted as a linear programming problem, and solved more efficiently than the QCQP problem of (24).

IV. NUMERICAL RESULTS

A single automotive radar chipset with N=3 transmit and M=4 receive antennas is considered in the simulation which can synthesize virtual sparse array with 12 elements using MIMO radar technique. The virtual sparse array geometry is first optimized to yield minimal PSL, as shown in Fig. 1. The optimal transmit and receiver antennas are located at $T_x = [1, 9, 18]\lambda/2$ and $R_x = [1, 3, 6, 7]\lambda/2$, respectively. The virtual sparse array aperture is $D = 11.5\lambda$. We first conduct Monte Carlo simulation in the interpolation region $\Psi = [-30^{\circ}, 30^{\circ}]$ that is discretized with step size of $\Delta\theta = 1^{\circ}$. The target angles are from -25° to 25° and dynamic range are from 15dB to 30dB. Chebyshev window with 30dB sidelobe suppression is adopted on the interpolated array measurements before 512-point fast Fourier transforms (FFTs) are carried out. To utilize the transform matrices obtained through different optimization approaches, the FFT spectra under different obtained transform matrices are combined by taking the minimal values for each FFT index to yield the final angle spectrum, $\mathbf{sp}_{\mathrm{full}}$.

Fig. 2 shows the angle spectrum comparison for signal-to-noise ratio (SNR) of 20dB. The sparse virtual array angle spectrum is obtained by performing FFT on the sparse array measurement filled with zeros in the positions of missing elements. It can be seen that the angle spectrum of the interpolated array has much higher

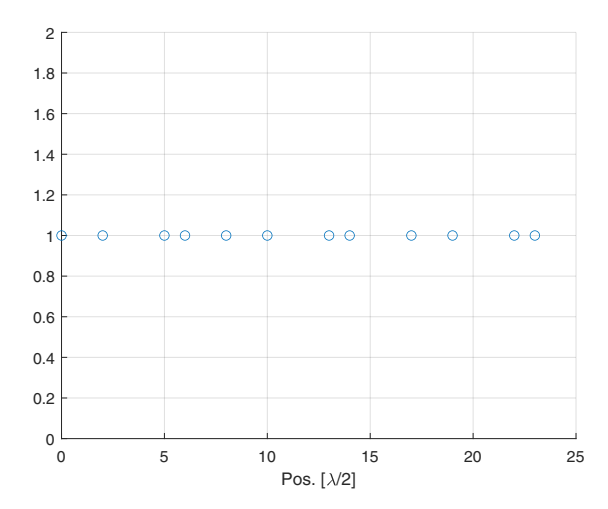


Fig. 1. Optimized virtual array geometry.

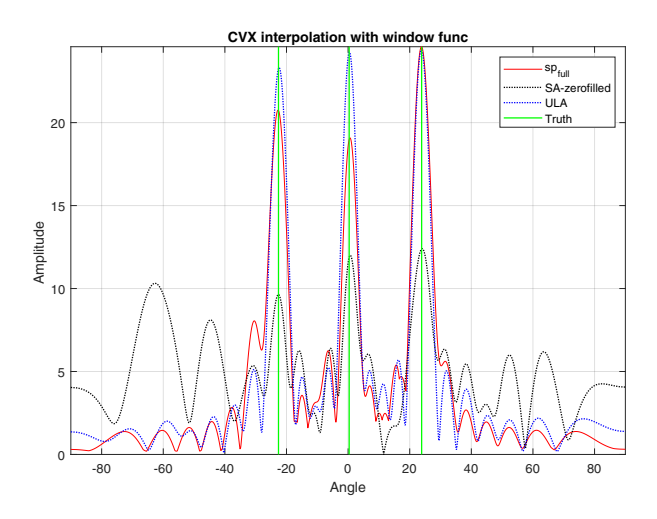
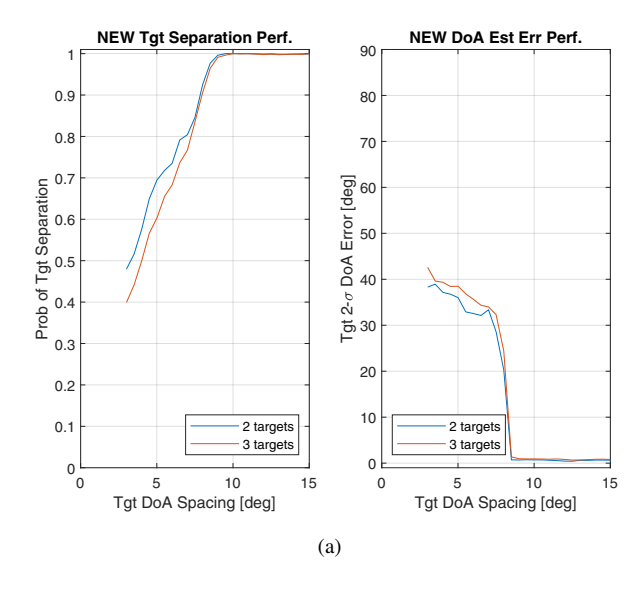


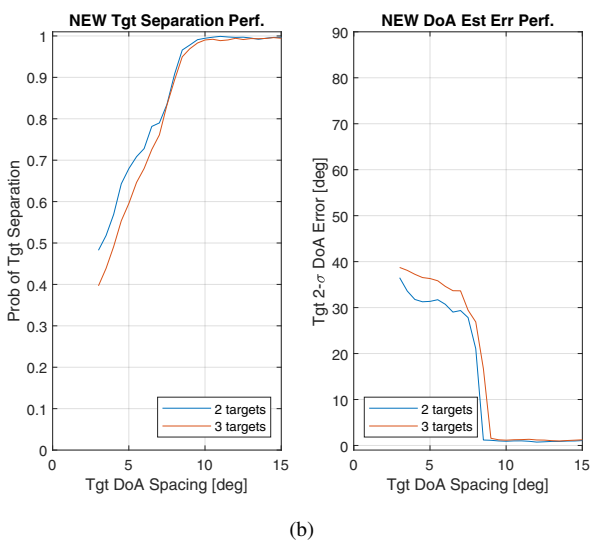
Fig. 2. Comparison of angle spectra at an SNR of 20dB, featuring three identical RCS targets at directions of -22 $^{\circ}$, 0 $^{\circ}$, and 24 $^{\circ}$.

amplitudes in the targets' directions, and lower sidelobe levels. The angle spectrum under full array is plotted for comparison.

We then verify the interpolation performance of transform matrix under different interpolation region sizes. Three interpolation regions of $\left[-25^{\circ},25^{\circ}\right],\ \left[-30^{\circ},30^{\circ}\right],$ and $\left[-35^{\circ},35^{\circ}\right]$ are tested on the same MIMO virtual array shown in Fig. 1. For a fair comparison, the performance of different-sized interpolation regions is evaluated on the same target set that includes 2 and 3 targets with different separations, respectively.

The performance comparison for different-size interpolation sectors are plotted in Fig. 3, where the probability of target separation and DOA estimation error are calculated by employing the key performance indicator (KPI). The initial stage of the KPI analysis involves identifying peaks within the estimated angle spectrum. The angle estimation error is averaged over Monte Carlo runs. In cases when there is an insufficient number of peaks, a random error is drawn from a uniform distribution spanning the field of view. An





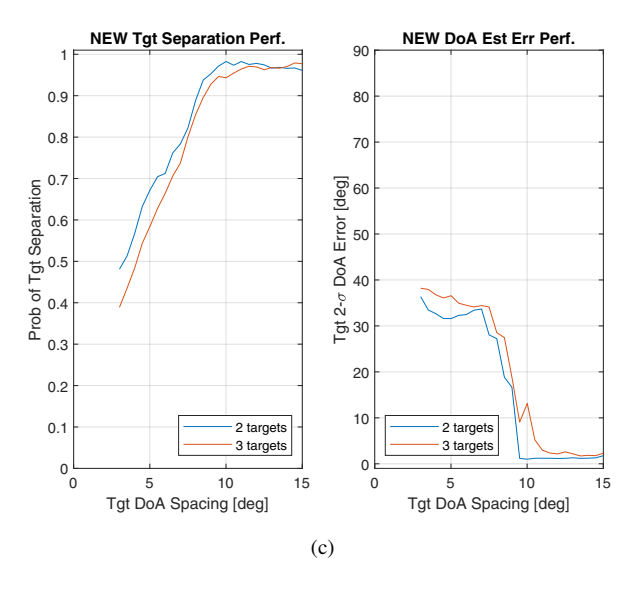


Fig. 3. Performance under different interpolation regions: (a) $\left[-25^{\circ}, 25^{\circ}\right]$; (b) $\left[-30^{\circ}, 30^{\circ}\right]$; (c) $\left[-35^{\circ}, 35^{\circ}\right]$.

approximated probability density function (PDF) is generated for each target, relying on the error histogram as a basis. To obtain the 2σ angle estimation error, the absolute values of angle-finding errors from all targets are computed and arranged in ascending order. The sorted absolute error vector serves as the x-coordinate values, while the normalized element indices of the error vector (increasing monotonically from $L_{\rm sample}^{-1}$ to 1, where $L_{\rm sample}$ is the number of error samples) act as the y-coordinate values. This arrangement facilitates the definition of the approximated cumulative density of function (CDF) for absolute angle-finding errors. In these plots, the 95% point is determined as the 2σ bound of the angle error. From Fig. 3, it is evident that the smallest interpolation region $\left[-25^{\circ},25^{\circ}\right]$ yields the best estimation performance. As the interpolation region expands, the performance tends to decrease. The larger the interpolation area, the poorer the estimation outcome tends to be.

V. CONCLUSION

This paper presented a comprehensive study on optimizing sparse array interpolation for automotive MIMO radar systems through the development of an optimal transform matrix. Various strategies has been investigated for designing an optimal transform matrix, enabling the effective interpolation of a virtual sparse array into a uniform linear array. A sector-based interpolation was introduced, allowing for more precise and targeted interpolation. This method also incorporates out-of-sector suppression to significantly reduce high sidelobes in adjacent sectors, enhancing overall system performance. The practical applicability and efficiency of the proposed virtual sparse array interpolation method were substantiated with numerical results, demonstrating its potential for significant improvements in automotive MIMO radar.

REFERENCES

- S. Sun, A. P. Petropulu, and H. V. Poor, "MIMO radar for advanced driver-assistance systems and autonomous driving: Advantages and challenges," *IEEE Signal Process. Mag.*, vol. 37, no. 4, pp. 98–117, 2020.
- [2] S. Sun and Y. D. Zhang, "4D automotive radar sensing for autonomous vehicles: A sparsity-oriented approach," *IEEE J. Sel. Topics Signal Process.*, vol. 15, no. 4, pp. 879–891, 2021.
- [3] M. Guo, Y. D. Zhang, and T. Chen, "DOA estimation using compressed sparse array," *IEEE Transactions on Signal Processing*, vol. 66, no. 15, pp. 4133–4146, 2018.
- [4] Y. Chi, L. L. Scharf, A. Pezeshki, and A. R. Calderbank, "Sensitivity to basis mismatch in compressed sensing," *IEEE Trans. Signal Process.*, vol. 59, no. 5, pp. 2182–2195, 2011.
- [5] L. Xu and S. Sun, "Coprime visible regions assisted angle unfolding for sparse ESPRIT," in *IEEE Radar Conference*, San Antonio, TX, May, 1-5, 2023.
- [6] P.-C. Chen and P. Vaidyanathan, "Rank properties of manifold matrices of sparse arrays," in 2021 55th Asilomar Conference on Signals, Systems, and Computers. IEEE, 2021, pp. 1628–1633.
- [7] P. Pal and P. P. Vaidyanathan, "Nested arrays: A novel approach to array processing with enhanced degrees of freedom," *IEEE Transactions on Signal Processing*, vol. 58, no. 8, pp. 4167–4181, 2010.
- [8] P. P. Vaidyanathan and P. Pal, "Sparse sensing with co-prime samplers and arrays," *IEEE Trans. Signal Process.*, vol. 59, no. 2, pp. 573–586, 2011.
- [9] S. Qin, Y. D. Zhang, and M. G. Amin, "Generalized coprime array configurations for direction-of-arrival estimation," *IEEE Transactions on Signal Processing*, vol. 63, no. 6, pp. 1377–1390, 2015.
- [10] J. Li, R. Wu, I.-T. Lu, and D. Ren, "Bayesian linear regression with Cauchy prior and its application in sparse MIMO radar," *IEEE Trans*actions on Aerospace and Electronic Systems, in press, 2023.
- [11] L. Xu, S. Sun, K. V. Mishra, and Y. D. Zhang, "Automotive FMCW radar with difference co-chirps," *IEEE Transactions on Aerospace and Electronic Systems*, in press, 2023.

- [12] G. K. Papageorgiou and M. Sellathurai, "Fast direction-of-arrival estimation of multiple targets using deep learning and sparse arrays," in ICASSP 2020-2020 IEEE International Conference on Acoustics, Speech and Signal Processing (ICASSP). IEEE, 2020, pp. 4632–4636.
- [13] R. Zheng, S. Sun, H. Liu, and T. Wu, "Deep-neural-network-enabled vehicle detection using high-resolution automotive radar imaging," *IEEE Transactions on Aerospace and Electronic Systems*, vol. 59, no. 5, pp. 4815–4830, 2023.
- [14] J. Youn, S. Ravindran, R. Wu, J. Li, and R. van Sloun, "Circular convolutional learned ISTA for automotive radar DOA estimation," in 2022 19th European Radar Conference (EuRAD), 2022, pp. 273–276.
- [15] Y. Hua and T. K. Sarkar, "Matrix pencil method for estimating parameters of exponentially damped/undamped sinusoids in noise," *IEEE Trans. Acoust., Speech, Signal Process.*, vol. 38, no. 5, pp. 814–824, 1990.
- [16] B. Friedlander and A. J. Weiss, "Direction finding for wide-band signals using an interpolated array," *IEEE Transactions on Signal Processing*, vol. 41, no. 4, pp. 1618–1634, 1993.
- [17] P. Hyberg, M. Jansson, and B. Ottersten, "Array interpolation and bias reduction," *IEEE Transactions on Signal Processing*, vol. 52, no. 10, pp. 2711–2720, 2004.
- [18] B. K. Lau, G. J. Cook, and Y. H. Leung, "An improved array interpolation approach to DOA estimation in correlated signal environments," in 2004 IEEE International Conference on Acoustics, Speech, and Signal Processing, vol. 2. IEEE, 2004, pp. ii–237.
- [19] T. K. Yasar and T. E. Tuncer, "Wideband DOA estimation for nonuniform linear arrays with Wiener array interpolation," in 2008 5th IEEE Sensor Array and Multichannel Signal Processing Workshop. IEEE, 2008, pp. 207–211.
- [20] C. Alcalde and Z. Li, "Detector device including a shifted multidimensional array of detector elements," U.S. Patent 10,725,152, July 28, 2020.
- [21] S. Zhang, A. Ahmed, Y. D. Zhang, and S. Sun, "DOA estimation exploiting interpolated multi-frequency sparse array," in 2020 IEEE 11th Sensor Array and Multichannel Signal Processing Workshop (SAM). IEEE, 2020, pp. 1–5.
- [22] S. Sun and Y. D. Zhang, "Multi-frequency sparse array-based massive MIMO radar for autonomous driving," in 2020 54th Asilomar Conference on Signals, Systems, and Computers, 2020, pp. 1167–1171.
- [23] S. Sun and A. P. Petropulu, "A sparse linear array approach in automotive radars using matrix completion," in *Proc. IEEE Int. Conf. Acoust.*, *Speech, Signal Process. (ICASSP)*, Barcelona, Spain, May 2020, pp. 8614–8618.
- [24] S. Zhang, A. Ahmed, Y. D. Zhang, and S. Sun, "Enhanced DOA estimation exploiting multi-frequency sparse array," *IEEE Transactions* on Signal Processing, vol. 69, pp. 5935–5946, 2021.
- [25] S. Sun, Y. Wen, R. Wu, D. Ren, and J. Li, "Fast forward-backward Hankel matrix completion for automotive radar DOA estimation using sparse linear arrays," in 2023 IEEE Radar Conference (RadarConf23). IEEE, 2023, pp. 01–06.
- [26] S. Sun, W. U. Bajwa, and A. P. Petropulu, "MIMO-MC radar: A MIMO radar approach based on matrix completion," *IEEE Trans. Aerosp. Electron. Syst.*, vol. 51, no. 3, pp. 1839–1852, 2015.
- [27] C. Greiff, F. Giovanneschi, and M. A. Gonzalez-Huici, "Matrix pencil method for DOA estimation with interpolated arrays," in 2020 IEEE International Radar Conference (RADAR). IEEE, 2020, pp. 566–571.
- [28] N. Jin and Y. Rahmat-Samii, "Advances in particle swarm optimization for antenna designs: Real-number, binary, single-objective and multiobjective implementations," *IEEE Trans. Antennas Propag.*, vol. 55, no. 3, pp. 556–567, 2007.
- [29] R. Zheng, S. Sun, W. Kuo, T. Abatzoglou, and M. Markel, "4D automotive radar exploiting sparse array optimization and compressive sensing," in 57th Asilomar Conference on Signals, Systems, and Computers, 2023.
- [30] M. Pesavento, A. B. Gershman, and Z.-Q. Luo, "Robust array interpolation using second-order cone programming," *IEEE Signal Processing Letters*, vol. 9, no. 1, pp. 8–11, 2002.
- [31] M. Grant and S. Boyd, "CVX: Matlab software for disciplined convex programming, version 2.1," http://cvxr.com/cvx, Mar. 2014.
- [32] H. Hung and M. Kaveh, "Focussing matrices for coherent signalsubspace processing," *IEEE Transactions on Acoustics, Speech, and Signal Processing*, vol. 36, no. 8, pp. 1272–1281, 1988.
- [33] M.-Y. Cao, S. A. Vorobyov, and A. Hassanien, "Transmit array interpolation for DOA estimation via tensor decomposition in 2-D MIMO radar," *IEEE Transactions on Signal Processing*, vol. 65, no. 19, pp. 5225–5239, 2017.